https://doi.org/10.5194/sand-2026-11
Preprint. Discussion started: 16 June 2026

SaND
Safety of Nuclear Waste Disposal
Discussions

Modelling contaminant transport of soil and landfills: A comparison study of three numerical codes

Marc Johnen[1], Roman Winter[2], Bernd Flemisch[2], Holger Class[2], Holger Seher[1], and Henrich Meyering[1]

[1]Gesellschaft für Anlagen- und Reaktorsicherheit (GRS) gGmbH, Cologne, 50667, Germany
[2]Institute for Modelling Hydraulic and Environmental Systems, University of Stuttgart, 70569 Stuttgart, Germany

Correspondence: Marc Johnen (marc.johnen@grs.de)

Abstract. The negligibly radioactive materials from a control area can be fed into further material cycles, to an incineration plant or disposed according to the type of clearance after clearance procedure, which is described in the German Radiation Protection Ordinance (Deutscher Bundestag, 2024b). The clearance values of the Radiation Protection Ordinance are based on the 10 µSv concept that limits the additional radiation exposure for the population or worker. In the past, analytical models were used to calculate radionuclide concentrations for groundwater path dose estimation. In this work, numerical groundwater models are used to simulate the distribution of radionuclides and provide spatial information on concentrations, which can be used as input data for dose estimation.

The transport processes of advection, diffusion, dispersion, sorption and decay are implemented in the simulation codes "distributed density-driven flow (d^3f++)" (Fein and Schneider, 1999; Fein, 2004), "Dune for Multiphase flow and transport (DuMu^x)" (Flemisch et al., 2011; Koch et al., 2021) and "Simulation of Processes in Groundwater (SPRING)" (delta h, 2024). To compare the codes and their implemented transport processes, a simple 2D column and a generic 2D landfill body were modelled. The study demonstrated a good agreement between the three computational codes, thereby strengthening trust in numerical modelling for future applications in dose estimation. The differences in the concentration breakthrough curves can be attributed to the differences in the implementation of initial conditions (IC) for saturation, the influence of dispersion in the different codes and the upwind methods, highlighting the sensitivity to these parameters and numerical solvers. Although minor discrepancies emerge in the results, the study demonstrates that the concentrations and the times of maximum concentration are largely comparable.

1 Introduction

With the nuclear phase-out, Germany decided to shut down all conventional nuclear power plants in Germany by 15th April 2023 at the latest (Deutscher Bundestag, 2022). Non-contaminated or slightly contaminated materials are produced in large quantities during the decommissioning and dismantling of nuclear facilities, or in significantly smaller quantities in medicine, research or the operation of nuclear facilities. After undergoing an officially approved clearance or release procedure regulated by the Radiation Protection Ordinance, these materials and objects are returned to the material cycle for recycling or further use or disposed of in a proper manner. In compliance with the clearance values from the German Radiation Protec-

https://doi.org/10.5194/sand-2026-11
Preprint. Discussion started: 16 June 2026

SaND
Safety of Nuclear Waste Disposal
Discussions

tion Ordinance (Deutscher Bundestag, 2024a), the 10 µSv concept of the International Atomic Energy Agency (IAEA) (1988) is not violated. By being below the clearance values, the decommissioning wastes are released by the responsible authority from radiation protection control. After release, the material can be disposed into the conventional waste and economic cycle. One option of disposal is the storage in landfills. Another option is the unrestricted clearance of land area on the former plant site. The regulatory requirements offer various clearance paths for decommissioning waste and exposure paths for dose estimation. From the inhalation of dust by an employee at landfill sites to the additional radiation exposure of a private individual through natural eating habits, various contamination paths are mapped. An important pathway in relation to the simulations here is the consumption of contaminated groundwater or the consumption of plants irrigated with contaminated water (Strahlenschutzkommission, 2006). In this work, the radionuclide concentration was simulated in accordance with regulatory requirements using numerical groundwater models. The outcome of radionuclide concentrations can be used for dose estimations. The focus was on a comparison of different numerical codes in order to gain additional confidence in the simulation of the radionuclide concentration using numerical groundwater models, as until now mostly analytical methods have been used to calculate the radionuclide concentration for the subsequent dose estimation.

2 Simulation Codes

In addition to the analytical calculations regarding the concentration of radionuclides in groundwater (Thierfeldt and Wörlen, 2004), only a few numerical simulations were carried out on groundwater flow and mass transport in connection with radionuclides (Merk, 2012; Seher et al., 2016; Artmann et al., 2020; Winter et al., 2022). The comparison carried out here is intended to highlight problems and differences in the implementation of numerical groundwater codes, where differences exist. Numerical groundwater models are used for different problems and in several work areas, as final disposal, groundwater salinisation, water management, e.g. for federal states or, at a regional level, for croplands or landfills or geothermal energy (Nordbotten et al., 2012; Ahusborde et al., 2015; Class et al., 2021; Rübel and Gehrke, 2022; Winter et al., 2022; Suilmann et al., 2025). With advancing technical development and increasing computing power, models can be made increasingly complex and comprehensive. Although a model is not capable of reproducing reality exactly, it creates the possibility to make well-founded estimates and gain a better understanding of the system. The three groundwater modelling codes used are briefly introduced below.

2.1 DuMu^x

"Dune for Multi-{phase, component, scale, physics, ...} flow and transport in porous media" (DuMu^x) is a research code written in C++ based on Dune (Bastian et al., 2021). The code is open source and freely available at https://dumux.org (Koch et al., 2021). Its main intention is to provide a sustainable and consistent framework for the implementation and application of porous media model concepts and constitutive relations. It has been successfully applied to gas storage scenarios, environmental remediation problems, transport of therapeutic agents through biological tissue, root-soil interaction, subsurface-atmosphere coupling, pore-network modelling, as well as flow and transport in fractured porous media.

https://doi.org/10.5194/sand-2026-11
Preprint. Discussion started: 16 June 2026

SaND Safety of Nuclear Waste Disposal Discussions

2.2 d^{3}f++

The "distributed density-driven flow" code (d^{3}f++) is a finite volume code (FVM) that was developed under the auspices of Gesellschaft für Anlagen- und Reaktorsicherheit (GRS) in cooperation with various universities in order to be able to deal with specific problems relating to groundwater flow with a focus on density-driven flow in large, complex areas (Fein and Schneider, 1999; Fein, 2004). The code is open source and freely available at https://github.com/UG4/app_d3f. d^{3}f++ can be and has already been used in the long-term safety analysis for the search for a repository, the modelling of the salinisation of near-surface aquifers on the coast, the modelling of fractures and fracture networks and the consideration of subrosion processes in the subsurface (Schneider et al., 2022; Flügge et al., 2024).

2.3 SPRING

The code "Simulation of Processes in Groundwater" (SPRING) was developed by delta h Ingenieurgesellschaft mbH and commercialised as conventional proprietary software (delta h, 2024). It combines the functions of geographical information systems (GIS) with numerical modelling. With the help of the finite element method (FEM), 1D, 2D, 2D/3D and 3D models can be created. SPRING allows the simulation of multi-dimensional groundwater flow, surface water, heat and mass transport models.

2.4 Flow and transport processes

The various codes implement the flow and mass transport processes in the same way for fluid flow and mass transfer. In DuMu^x, a two-phase flow can be modelled, which is not possible in d^{3}f++ and SPRING. Due to this difference, identical discretisation and parametrization is not possible without converting pressures within the model domain, and this may account for minor differences in the results. Firstly, the mathematical implementations for the transport equations are described, afterwards the results of the comparison of the equations of the three codes are explained. For the mass balance of water, Richards equation is used (Šimůnek et al., 2003; Nayagum et al., 2004). It is a simplification of the two-phase equations under the assumption of an infinitely mobile gaseous phase. This assumption implies that the pressure of air is a static constant value over the whole domain of interest and that, therefore, mass conservation only needs to be considered for water w, namely,

$$\frac{\partial(\varrho_w \phi S_e)}{\partial t} + \nabla \cdot (\varrho_w \mathbf{v}_f) - \varrho_w q_w = 0. \tag{1}$$

Above, ϕ indicates the dimensionless porosity, ϱ_w the water phase density in kilogram per cubic meter, S_e the effective water saturation, the Darcy velocity $\mathbf{v}_f$ in meter per second, and q_w the volumetric source term in per second. This formulation is equivalent to a storage term written in terms of the volumetric water content θ, using the relation given in Eq. (4). The momentum balance is used to calculate the velocity in Eq. (1) after Darcy, namely,

$$\mathbf{v}_f = -\frac{k}{\mu} \nabla p, \tag{2}$$

with the permeability k in square meter, the dynamic viscosity μ in Pascal second and the pressure gradient ∇p in Pascal per meter. According to van Genuchten (1980), the effective saturation S_e (dimensionless) depends on the capillary pressure p_c in

https://doi.org/10.5194/sand-2026-11
Preprint. Discussion started: 16 June 2026

SaND
Safety of Nuclear Waste Disposal
Discussions

Pascal as follows

$$S_e(p_c) = [1 + (\alpha p_c)^n]^{-m}, \qquad m = 1 - \frac{1}{n}, \tag{3}$$

with material parameters α per centimetre, n and m which have to be estimated from soil parameters and $n > 1$. The effective saturation S_e describes the hydraulic state of the pore space and is used for the determination of capillary pressure and flow properties. The effective saturation is defined in terms of the volumetric water content as

$$S_e = \frac{\theta - \theta_r}{\theta_s - \theta_r}, \tag{4}$$

where θ_r denotes the residual water content and θ_s the saturated water content, both in cubic centimetre per cubic centimetre. Combining Eq. (3) and Eq. (4), the volumetric water content can be written as

$$\theta(p_c) = \theta_r + (\theta_s - \theta_r)\,[1 + (\alpha p_c)^n]^{-m} \tag{5}$$

For the transport of dissolved substances in the fluid, further processes are taken into account. These include advection, diffusion, dispersion and adsorption. The following is a brief description of the mass transport processes based on the equations mentioned in Koch et al. (2021)

$$\underbrace{\frac{\partial(\varrho_w \theta X^\kappa)}{\partial t}}_{\text{Storage + Adsorption}} + \underbrace{\nabla \cdot (\varrho_w X^\kappa \mathbf{v}_f)}_{\text{Advection}} - \nabla \cdot (\varrho_w (\underbrace{D^\kappa_{\text{eff}}}_{\text{Diffusion}} + \underbrace{D^\kappa_{\text{disp}}}_{\text{Dispersion}}) \nabla X^\kappa) = q, \tag{6}$$

with θ the volumetric water content and the mass fraction X^κ in kilogram per kilogram. The effective diffusion coefficient in Eq. (6) is defined as

$$D^\kappa_{\text{eff}} = \theta \tau D^\kappa_w, \tag{7}$$

with tortuosity τ and the binary diffusion coefficient D^κ_w. In unsaturated porous media, solute transport occurs only within the water-filled pore space. For the dispersion in Eq. (6), the approach after Scheidegger (1961) is used, namely,

$$D^\kappa_{\text{disp}} = (\alpha_l - \alpha_t) \frac{\mathbf{v}_f \mathbf{v}_f^T}{|\mathbf{v}_f|} + \alpha_t |\mathbf{v}_f| \mathbf{I}. \tag{8}$$

Sorption, the chemical retardation of substances on the surface of solid material, considers the change of adsorbed mass

$$\frac{\partial(\varrho_s X^\kappa_s)}{\partial t} \tag{9}$$

with the solid rock density ϱ_s in kilogram per cubic meter. To describe the sorption, we choose the commonly used K_d-approach. The partition coefficient K_d describes the relation between the concentration X^κ dissolved in the fluid and the concentration X^κ_s adsorbed on the solid matrix as

$$K_d = \frac{X^\kappa_s}{X^\kappa}. \tag{10}$$

https://doi.org/10.5194/sand-2026-11
Preprint. Discussion started: 16 June 2026

SaND Safety of Nuclear Waste Disposal Discussions

Sorption coefficients can vary over several orders of magnitude, depending on the radionuclide, soil characteristics, the oxidation state, pH of the soil and redox conditions. It is therefore hard to estimate the correct sorption coefficient without measurements for the exact conditions (United States Environmental Protection Agency (US EPA), 1999; Stockmann et al., 2017; Noseck et al., 2018). A value of $K_d = 1 \times 10^{-3}\,\mathrm{m^3\,kg^{-1}}$ represents a medium sorbing radionuclide (Sheppard and Thibault, 1990; Thierfeldt and Wörlen, 2004; Artmann et al., 2020).

The sorbed concentration X_s^κ in Eq. (9) is substituted by $X_s^\kappa = K_d X^\kappa$. The resulting equation is

$$\frac{\partial(\theta X^\kappa + (1-\phi)\varrho_s K_d X^\kappa)}{\partial t} + \nabla\cdot(X^\kappa \mathbf{v}_f) - \nabla\cdot\left(\left(\theta\tau D_w^\kappa + (\alpha_l - \alpha_t)\frac{\mathbf{v}_f\mathbf{v}_f^T}{|\mathbf{v}_f|} + \alpha_t|\mathbf{v}_f|\mathbf{I}\right)\nabla X^\kappa\right) = q. \tag{11}$$

The effective saturation S_e is solely used to determine flow properties such as capillary pressure and relative permeability, whereas solute transport is governed by the volumetric water content θ. ϱ_s denotes the solid density per bulk volume. For a more detailed insight into the implementation of the transport processes of the individual codes, the reader is referred to delta h (2024); LH2 (2024); Fein and Schneider (1999); Fein (2004).

2.5 Code comparison

In the following, the governing transport equations implemented in the different numerical codes are compared. While the formulations presented in the respective code documentations appear substantially different at first glance, these differences primarily arise from varying choices of state variables and notations. By consistently mapping the variables and writing the equations in a unified form, it becomes evident that the underlying physical implementation is largely equivalent. The comparison therefore focuses on identifying and discussing the remaining differences, which are related to specific modeling assumptions and implementation details. The full transport equation in SPRING is documented as:

$$\frac{\partial(\theta X^\kappa + (1-\phi)\varrho_s K_d X^\kappa)}{\partial t} + \nabla\cdot(X^\kappa\theta\mathbf{v}) - \nabla\cdot(\theta(D_w^\kappa\mathbf{I} + D_d)\nabla X^\kappa) = q, \tag{12}$$

with the average interstitial velocity v, which is defined in an unsaturated porous medium as:

$$\mathbf{v} = \frac{1}{\theta}\mathbf{v}_f. \tag{13}$$

where v_f denotes the Darcy flux, while v represents the average interstitial velocity. The transport equation in d^{3}f++ is described as (Fein and Schneider, 1999; Fein, 2004)

$$\frac{\partial(\theta X^\kappa + (1-\phi)\varrho_s K_d X^\kappa)}{\partial t} + \nabla\cdot(X^\kappa \mathbf{v}_f) - \nabla\cdot\left(\left(\theta D_w^\kappa\mathbf{I} + (\alpha_l - \alpha_t)\frac{\mathbf{v}_f\mathbf{v}_f^T}{|\mathbf{v}_f|} + \alpha_t|\mathbf{v}_f|\mathbf{I}\right)\nabla X^\kappa\right) = q. \tag{14}$$

During the comparison process, disparities in the differential equations were identified. The disparities between the equations in DuMu^x compared to SPRING and d^{3}f++ are denoted in red, while disparities between DuMu^x and d^{3}f++ compared to SPRING are indicated in green:

$$\frac{\partial(\theta X^\kappa + (1-\phi)\varrho_s K_d X^\kappa)}{\partial t} + \nabla\cdot(X^\kappa \mathbf{v}_f) - \nabla\cdot\left(\left(\theta\tau D_w^\kappa\mathbf{I} + (\alpha_l - \alpha_t)\frac{\mathbf{v}_f\mathbf{v}_f^T}{|\mathbf{v}_f|} + \alpha_t|\mathbf{v}_f|\mathbf{I}\right)\nabla X^\kappa\right) = q. \tag{15}$$

https://doi.org/10.5194/sand-2026-11
Preprint. Discussion started: 16 June 2026

SaND Safety of Nuclear Waste Disposal Discussions

The source code for the DuMu^x model was modified to accommodate certain discrepancies. Specifically, the sorption term was expanded to encompass the term $(1-\phi)$, which is not implemented this way in the DuMu^x source code normally. It should be noted that the inclusion of the factor $(1-\phi)$ in the sorption storage term is not indicative of a different physical model, but rather results from different definitions of the sorbed concentration used in the respective codes. In particular, the necessity of explicitly scaling the sorbed mass with the solid volume fraction depends on whether the sorbed concentration is defined per unit bulk volume or per unit solid mass. The modification applied in DuMu^x was therefore required to ensure consistency of variable definitions and a common volumetric interpretation of the governing equations across all codes. The tortuosity was defined as 1 (default value in DuMu^x is 0.5), d^{3}f++ uses a default value of 1 and SPRING has no tortuosity in the code documentation. These adjustments were made to allow a direct comparison of the three codes.

3 Model description

3.1 Soil model

A simple quasi-1D model of a 9 meter high soil profile was developed. The first meter at the model surface represents contaminated soil, which is excavated at a potential nuclear power plant site and deposited at a landfill. Percolating rainwater leaches the pollutants from the soil and transports them further into the ground. With its simple generic quasi-1D structure, the soil model provides a good basis for code comparison. No stochastic heterogeneous parameter distributions were applied in the soil layers. The transport simulations are carried out to determine the clearance pathway after StrlSchV 2024 Column 7 "specific clearance of soil in Bequerel per gram".

The model is $9\,\mathrm{m}$ high, $1\,\mathrm{m}$ wide and is divided into the three areas as depicted in Figure 1: the contaminated soil, the unsaturated and the saturated zone. At the top of the model a steady Neumann boundary condition (BC) with an inflow rate of $0.25\,\mathrm{m\,yr^{-1}}$ is set and at the base of the model a Dirichlet BC of $9\,\mathrm{m}$ (saturated model cases) or $5\,\mathrm{m}$ (unsaturated model cases) is applied. The lateral model boundaries are no-flow boundaries. The unsaturated and saturated zones differ only in the BC due to the different Dirichlet BC for the saturated and unsaturated cases, not in any material characteristics. Only the permeability of the contaminated soil layer is different compared to the underlying layers. Effective porosity and rock density remain constant in the model, all material properties are shown in Table 1.

Table 1. Material parameters for the soil model in Figure 1.

Layer	Height [m]	Permeability [$\mathrm{m^2}$]	Porosity [-]	Rock density [$\mathrm{kg\,m^{-3}}$]
Contaminated soil	1	1.3×10^{-11}	0.2	1800
Vadose zone	3	1.3×10^{-12}	0.2	1800
Aquifer	5	1.3×10^{-12}	0.2	1800

https://doi.org/10.5194/sand-2026-11
Preprint. Discussion started: 16 June 2026

SaND
Safety of Nuclear Waste Disposal
Discussions

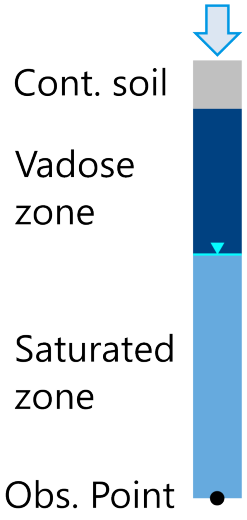

Figure 1. Schematic setup of the soil model. $1\,\mathrm{m}$ contaminated soil (grey), $3\,\mathrm{m}$ vadose zone due to BC (dark blue) and $5\,\mathrm{m}$ saturated zone (light blue). Arrow represents a Neumann BC with a steady inflow rate of $0.25\,\mathrm{m\,yr^{-1}}$. At the model basis an observation point is located for the concentration comparison of the codes.

The initial saturation and pressure conditions are simulated with a transient flow model, which runs until a steady state is reached. So the saturation within the soil column is already stationary at the first time step of the transport simulation. The saturation conditions in the model are strongly dependent on the van Genuchten parameters (van Genuchten, 1980) for the unsaturated flow after the Richards equation with α ($1.4 \times 10^{-3}\,\mathrm{m^2\,N^{-1}}$) as reciprocal of the water inlet pressure, n (3 [-]) the pore space index, $S_{e,r}$ (1.0 [-]) the water content and $S_{n,r}$ (0.2 [-]) the residual water content. The van Genuchten parameters used are valid for well sorted sands (Benson et al., 2014).

The initial concentration in the $1\,\mathrm{m}$ thick contaminated soil is $1\,\mathrm{kg\,kg^{-1}}$, and $0\,\mathrm{kg\,kg^{-1}}$ for the rest of the soil column. The infiltrating rainwater has a concentration of $0\,\mathrm{kg\,kg^{-1}}$ so the maximum mass is already entered at the start of the simulation and no additional tracer is given into the model afterwards. The fluid density and viscosity are fixed with values of $1 \times 10^{3}\,\mathrm{kg\,m^{-3}}$ and $1 \times 10^{-3}\,\mathrm{kg\,m^{-1}\,s^{-1}}$.

To identify possible differences between the codes, ten different parameter sets were selected for the soil model. These ten simulation cases were run for both saturated and unsaturated soil conditions. The parametrization is described in Table A1. The first simulation case considers only advection, the other three consider advection with dispersion, diffusion, and sorption, respectively. In the remaining cases, the parameters were varied without aiming to completely cover their parameter spectrum. To compare the model results, the saturation and pressure distribution are plotted as well as the concentration breakthrough curve at the coordinates (0, 0) over time.

https://doi.org/10.5194/sand-2026-11
Preprint. Discussion started: 16 June 2026

SaND
Safety of Nuclear Waste Disposal
Discussions

3.2 Landfill model

The transport simulations of the 2D landfill are carried out to determine the clearance pathway after StrlSchV 2024 Column 10 "Specific clearance of solid materials up to $1000\,\mathrm{Mg\,yr^{-1}}$ for disposal on landfills in Becquerel per gram".

The model includes a $300\,\mathrm{m}$ wide and $25\,\mathrm{m}$ high landfill. Underneath is a $0.5\,\mathrm{m}$ thick drainage layer, followed by a $1\,\mathrm{m}$ thick geological barrier according to DepV. Below these three compartments a $20\,\mathrm{m}$ thick aquifer with a total length of $850\,\mathrm{m}$ is located. In order to reduce numerical boundary effects at the transition between the geological barrier and aquifer, the landfill is not directly located at the model edge but is oriented slightly towards the center (Figure 2).

The model geometry has a gradient of $0.025\,\mathrm{m\,m^{-1}}$ to represent a hydraulic gradient in the aquifer (table C1). This gradient is also present in the landfill geometry. A steady Neumann BC with an inflow rate of $0.25\,\mathrm{m\,yr^{-1}}$ is applied at the model surface. A Dirichlet BC with a water column height of $14\,\mathrm{m}$ is applied at the left and right model boundaries. The sides of the landfill, the drainage and the geological barrier are closed with a no-flux boundary. Infiltration water from the surface of the landfill is not able to drain out of the model at this point. This results in higher concentrations in the geological barrier and the aquifer and therefore can be regarded as conservative for the groundwater path, as the whole input mass is transported through the geological barrier into the groundwater instead of being collected at the landfill base and later treated in a sewage treatment plant.

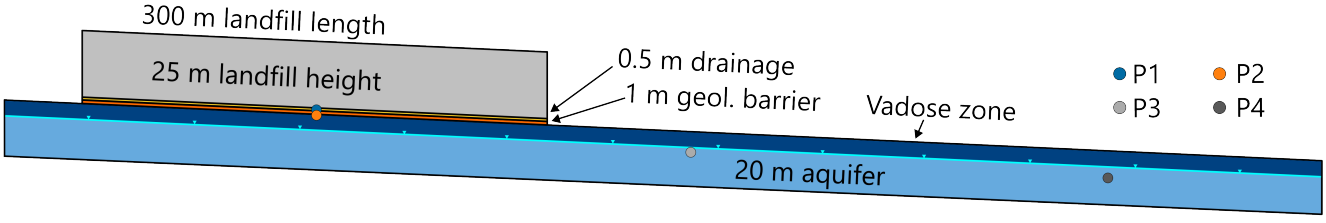

Figure 2. Schematic setup of the landfill model (y-axis two times exaggerated). $25\,\mathrm{m}$ height landfill (grey) with a $0.5\,\mathrm{m}$ drainage layer, a $1\,\mathrm{m}$ thick geological barrier. A $20\,\mathrm{m}$ thick aquifer adjoins to the geological barrier with a Dirichlet BC of $14\,\mathrm{m}$ defining a vadose zone of $6\,\mathrm{m}$ at the start of the flow simulations. Several observation points (P1 to P4) are located in the model for the concentration comparison of the codes.

The initial concentration in the landfill is $1\,\mathrm{kg\,kg^{-1}}$ over the whole landfill height of $25\,\mathrm{m}$. The remaining compartments have an initial concentration of $0\,\mathrm{kg\,kg^{-1}}$. The infiltrating rainwater has a concentration of $0\,\mathrm{kg\,kg^{-1}}$. Initial saturation and pressure conditions are simulated with a transient flow model until a steady state. Viscosity, fluid density and van Genuchten parameters equal the values for the soil model.

Porosity and rock density remain constant across the different layers. The permeability values vary in relation to the assumed permeability for landfill material, a hydraulically well connected aquifer (conservative) and the required permeability values for the geological barrier with $1 \times 10^{-9}\,\mathrm{m\,s^{-1}}$ after DepV. The material properties for the different layers are shown in Table 2. Several simulations were performed, but due to repetitive results, only three are described in detail here. The parameters of

https://doi.org/10.5194/sand-2026-11
Preprint. Discussion started: 16 June 2026

SaND
Safety of Nuclear Waste Disposal
Discussions

Table 2. Material parameters for the different layers of the landfill model.

Layer	Height [m]	Permeability [m^2]	Porosity [-]	Rock density [$kg\,m^{-3}$]
Landfill	25	1.3×10^{-12}	0.2	1800
Drainage	0.5	1.3×10^{-11}	0.2	1800
Barrier	1	1.3×10^{-16}	0.2	1800
Vadose zone	6	1.3×10^{-12}	0.2	1800
Aquifer	14	1.3×10^{-12}	0.2	1800

these simulation cases are shown in Table B1. To compare the model results, the concentration breakthrough curves at the coordinates, shown in Table 3, are plotted over time.

Table 3. Observation points for concentration evaluation of the landfill model.

Observation point	X-coordinate [m]	Y-coordinate [m]
P1	200	37.25
P2	200	36.25
P3	440	21.60
P4	707	14.00

4 Results

4.1 Soil model

4.1.1 Tracer transport times - saturated simulation cases

For the evaluation, several simulation cases are shown in one figure. However, due to the large number of simulation cases, not all breakthrough curves were plotted in one diagram to ensure readability. The figures shown in this section originate from the simulations for the saturated soil model. The first four simulation cases show the individual transport processes and possible differences in the codes. Apart from advection, no other transport process is taken into account for simulation case 1. The results show identical concentration curves for all three codes (Figure 3). This also applies to simulation cases 3 (diffusion) and 4 (sorption). For simulation case 2 (dispersion), stronger dispersion results in a lower peak concentration for DuMu^x. The origin of this effect could not be identified, as the mathematical description of the dispersion is the same in the codes. An in-depth search in the code also did not reveal any bug leading to this difference.

With the boundary conditions and parameters used, dispersion leads to a stronger distribution of the concentration relative to the influence of the diffusion flux. In contrast to dispersion and diffusion, sorption does not lead to a stronger distribution of the concentration, but to a retardation of the radionuclides on the material surfaces in the porous medium. With a sorption

https://doi.org/10.5194/sand-2026-11
Preprint. Discussion started: 16 June 2026

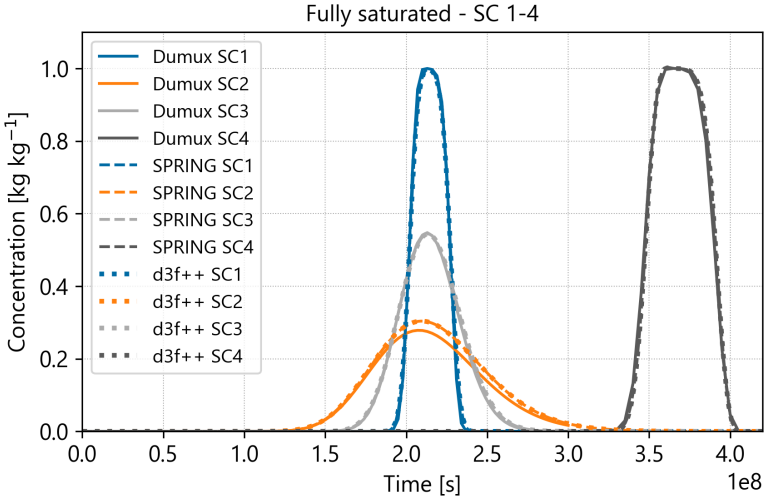

Figure 3. Concentration breakthrough curves for the simulation cases 1 to 4 (saturated cases) for the three different Codes DuMu^{x} (solid line), d^{3}f++ (dotted line) and SPRING (dashed line). Blue curve: advective transport; orange curve: advection and dispersion; grey curve: advection and diffusion; black curve: advection and sorption.

coefficient of $1 \times 10^{-4}\,\mathrm{m^3\,kg^{-1}}$, the pollutant takes almost twice as long to be transported to the observation point at the model base as without sorption.

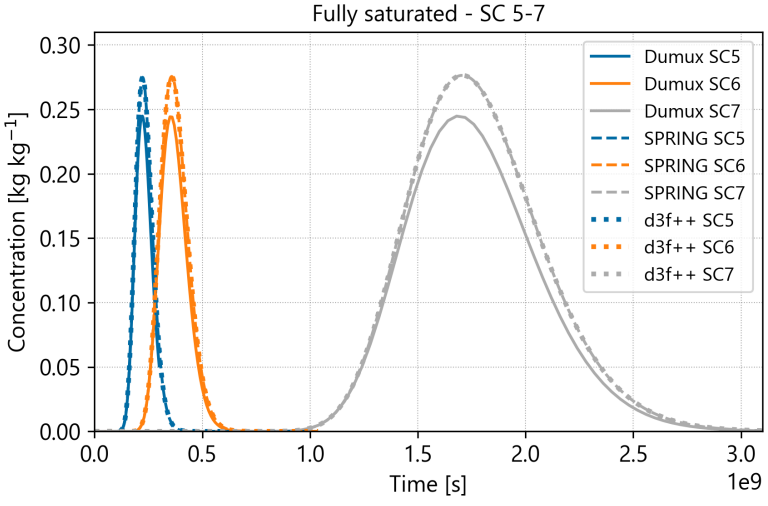

Figure 4. Concentration breakthrough curves for the simulation cases 5 to 7 (saturated cases) for the three different Codes DuMu^{x} (solid line), d^{3}f++ (dotted line) and SPRING (dashed line). All cases use the same dispersion ($0.1\,\mathrm{m}$) and diffusion coefficient ($1 \times 10^{-9}\,\mathrm{m^2\,s^{-1}}$) and vary in the sorption coefficients. Blue curve: $1 \times 10^{-5}\,\mathrm{m^3\,kg^{-1}}$; orange curve: $1 \times 10^{-4}\,\mathrm{m^3\,kg^{-1}}$; grey curve: $1 \times 10^{-3}\,\mathrm{m^3\,kg^{-1}}$.

https://doi.org/10.5194/sand-2026-11
Preprint. Discussion started: 16 June 2026

SaND Safety of Nuclear Waste Disposal Discussions

The influence of variable sorption coefficients, which correspond to the value range for some radionuclides, are shown in simulation cases 5 to 7 with the same dispersion coefficient and diffusion coefficients (Figure 4). The processes of dispersion and diffusion result in a stronger distribution of the pollutant in the model compared to purely advective transport. The breakthrough curves of all codes show good agreement, solely the effect of the stronger dispersion in DuMu^x differentiates the concentrations in the range of $0.25\,\mathrm{kg\,kg^{-1}}$. With increasing sorption, the transport through the model is retarded considerably. With a sorption coefficient of $1 \times 10^{-3}\,\mathrm{m^3\,kg^{-1}}$, it takes almost $50\,\mathrm{yr}$ to reach the maximum concentration of $0.27\,\mathrm{kg\,kg^{-1}}$.

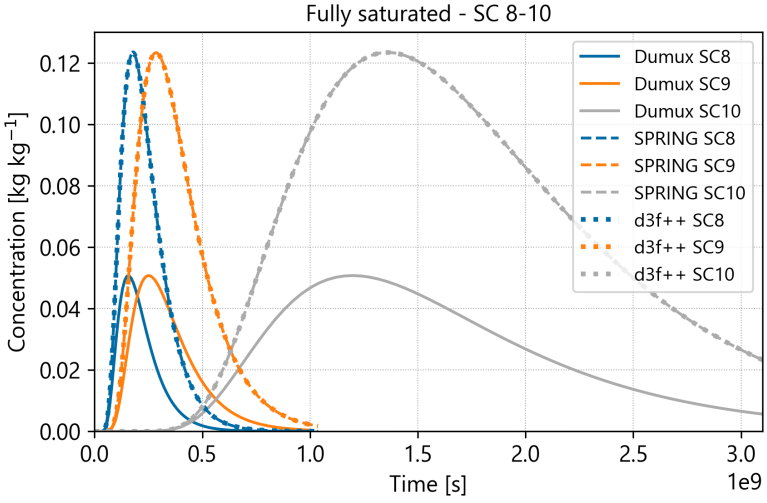

Figure 5. Concentration breakthrough curves for the simulation cases 8 to 10 (saturated cases) for the three different Codes DuMu^x (solid line), d^{3}f++ (dotted line) and SPRING (dashed line). All cases use the same dispersion ($1\,\mathrm{m}$) and diffusion coefficient ($1 \times 10^{-9}\,\mathrm{m^2\,s^{-1}}$) and vary in the sorption coefficients. Blue curve: $1 \times 10^{-5}\,\mathrm{m^3\,kg^{-1}}$; orange curve: $1 \times 10^{-4}\,\mathrm{m^3\,kg^{-1}}$; grey curve: $1 \times 10^{-3}\,\mathrm{m^3\,kg^{-1}}$.

Increasing the dispersion coefficients by factor 10 results in greater differences between the breakthrough curves of d^{3}f++ and SPRING compared to DuMu^x. The DuMu^x results show an earlier and lower concentration maximum for the simulation cases 8 to 10 (Figure 5). For d^{3}f++ and SPRING the peaks are at $0.12\,\mathrm{kg\,kg^{-1}}$, for DuMu^x at $0.05\,\mathrm{kg\,kg^{-1}}$. These simulation cases show that higher dispersion coefficients lead to a stronger discrepancy between the concentration breakthrough curves for the codes.

4.1.2 Tracer transport times - unsaturated simulation cases

Simulation cases 11 to 20 represent the unsaturated simulations of the soil model. As with the saturated simulations, the breakthrough curves are largely consistent for all codes, as for the simulation cases 1 to 4 (Figure 6). There is a temporal offset in the concentration maxima between the codes. The temporal offset is negligible within the scope of the model size and the simulation period. The concentration peak is lower in the unsaturated simulations compared to the saturated cases. This is the case due to the changes in the water content compared to the saturated tone and change the transport behaviour

https://doi.org/10.5194/sand-2026-11
Preprint. Discussion started: 16 June 2026

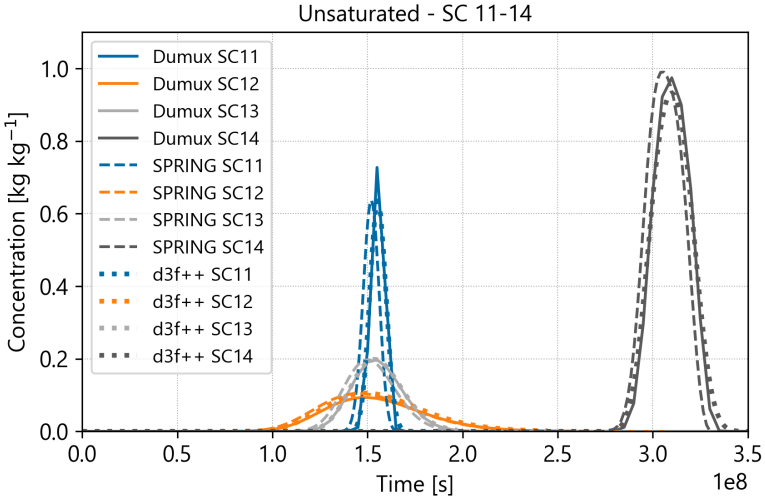

Figure 6. Concentration breakthrough curves for the simulation cases 11 to 14 (unsaturated cases) for the three different Codes DuMu^x (solid line), d^{3}f++ (dotted line) and SPRING (dashed line). Blue curve: advective transport; orange curve: advection and dispersion; grey curve: advection and diffusion; black curve: advection and sorption.

in the unsaturated zone. The concentration curves for DuMu^x and d^{3}f++ show slight differences. The DuMu^x simulations show a higher concentration peak in SC11 and SC14, as well as flatter concentration gradients at the base of the concentration curves (at low concentrations). The SPRING simulations show similar concentration curve profiles. For all simulation cases using SPRING, the concentrations reach the observation points slightly earlier. With the change to the unsaturated cases, the differences in concentration due to dispersion (orange curve (SC2) in Figure 3) is less visible in simulation case 12. Transport through the soil column is accelerated by the lower saturation compared to the saturated cases. The lower saturation means less water mass at the same flow rate. This leads to a higher velocity per volume and faster transport and stronger mixing with lower concentrations. For SC1-4 and SC11-14 the time difference between the concentration peak is around $1.6\,\mathrm{yr}$ due to the saturated or unsaturated conditions.

The concentration maxima in the model with unsaturated zone are at lower concentrations compared to the simulations in the fully saturated model for simulation case 15 and 16, depending on the sorption coefficient and the saturation (Figure 7). In unsaturated simulations, the amount of solute initially stored in the porous medium depends strongly on the sorption coefficient. A lower sorption coefficient implies less mass retained in the solid matrix under unsaturated conditions. This results in lower concentrations observed at the observation point, even though the timing of breakthrough remains largely unaffected from the unsaturated conditions. With lower sorption coefficients ($1 \times 10^{-4}\,\mathrm{m^3\,kg^{-1}}$) the concentrations are instead of $0.27\,\mathrm{kg\,kg^{-1}}$ at $0.19\,\mathrm{kg\,kg^{-1}}$ in d^{3}f++ and SPRING and $0.11\,\mathrm{kg\,kg^{-1}}$ with a sorption coefficient of $1 \times 10^{-5}\,\mathrm{m^3\,kg^{-1}}$ comparing the saturated and unsaturated cases. So the sorption coefficient and the consideration of unsaturated conditions impact the height of the maximum concentration peak. For the simulation cases (SC17) with sorption coefficients $1 \times 10^{-3}\,\mathrm{m^3\,kg^{-1}}$, a higher concentration

https://doi.org/10.5194/sand-2026-11
Preprint. Discussion started: 16 June 2026

SaND
Safety of Nuclear Waste Disposal
Discussions

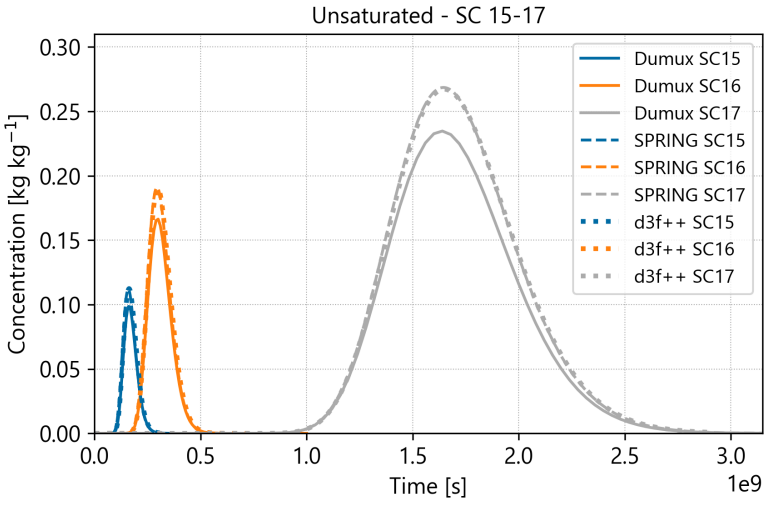

Figure 7. Concentration breakthrough curves for the simulation cases 15 to 17 (unsaturated cases) for the three different Codes DuMu^x (solid line), d^{3}f++ (dotted line) and SPRING (dashed line). All cases use the same dispersion ($0.1\,\mathrm{m}$) and diffusion coefficient ($1 \times 10^{-9}\,\mathrm{m^2\,s^{-1}}$) and vary in the sorption coefficients. Blue curve: $1 \times 10^{-5}\,\mathrm{m^3\,kg^{-1}}$; orange curve: $1 \times 10^{-4}\,\mathrm{m^3\,kg^{-1}}$; grey curve: $1 \times 10^{-3}\,\mathrm{m^3\,kg^{-1}}$.

is simulated in the unsaturated case compared to the saturated case in DuMu^x. This tendency is not recognizable for d^{3}f++ and SPRING. With $1 \times 10^{-5}\,\mathrm{m^3\,kg^{-1}}$ (SC15) and $1 \times 10^{-4}\,\mathrm{m^3\,kg^{-1}}$ (SC16), the concentration curves of DuMu^x, d^{3}f++ and SPRING overlap and do not diverge, as was the case in the saturated model.

Higher dispersion coefficients in the simulation cases 18 to 20 again show a reduced maximum concentration in DuMu^x compared to d^{3}f++ and SPRING (Figure 8), as it was in the saturated cases (Figure 5). The combination of a higher dispersion coefficient and a small element length in the numerical grid lead to a significant mixing of the concentration in the saturated and unsaturated simulation using DuMu^x.

4.2 Landfill model

In the landfill model, the breakthrough curves are created at four coordinates (Table 3). The first two points P1 and P2 are located in the center below the landfill body directly above and below the geological barrier (Figure 2). Point P3 is located in the nearby downstream of the landfill and point P4 is located at a distance of $500\,\mathrm{m}$ from the center of the landfill. Differences in the flow and transport processes and their implementation have already been considered in the soil model, so that simulation cases without dispersion and diffusion were not used here. The simulation cases differ in the varying sorption coefficients, representative of the sorption behavior of different radionuclides, and the change in dispersion coefficients. As the dispersion in the soil model had a clear effect on the concentration curves, the influence should also be investigated in the landfill model. Simulation case 1 takes into account advection, dispersion and diffusion. Sorption is not considered; the sorption coefficient is $0\,\mathrm{m^3\,kg^{-1}}$. The tracer is transported by the assumed groundwater infiltration rate to the base of the landfill. The concentration

https://doi.org/10.5194/sand-2026-11
Preprint. Discussion started: 16 June 2026

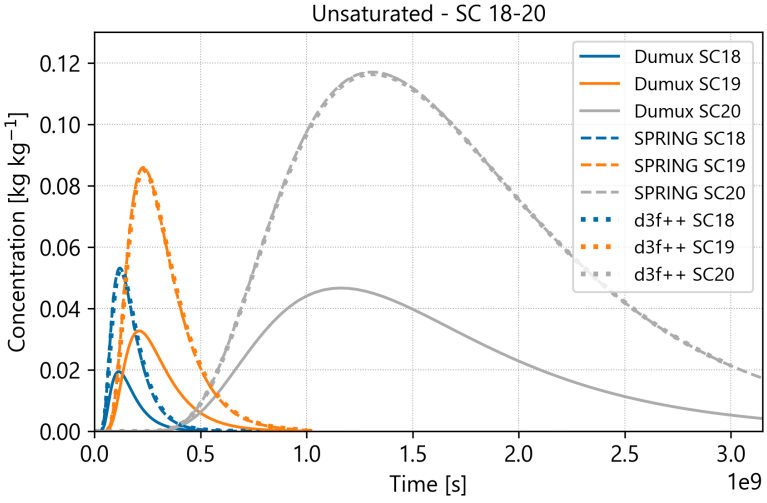

Figure 8. Concentration breakthrough curves for the simulation cases 18 to 20 (unsaturated cases) for the three different Codes DuMu^{x} (solid line), d^{3}f++ (dotted line) and SPRING (dashed line). All cases use the same dispersion (1 m) and diffusion coefficient ($1 \times 10^{-9}\,\mathrm{m^2\,s^{-1}}$) and vary in the sorption coefficients. Blue curve: $1 \times 10^{-5}\,\mathrm{m^3\,kg^{-1}}$; orange curve: $1 \times 10^{-4}\,\mathrm{m^3\,kg^{-1}}$; grey curve: $1 \times 10^{-3}\,\mathrm{m^3\,kg^{-1}}$.

at the observation point above the geological barrier quickly rises to the initial concentration within the landfill of $1\,\mathrm{kg\,kg^{-1}}$ in the area of the geological barrier (Figure 9). Without drainage water extraction in the model, the water is pushed through the landfill body towards the groundwater. All the tracer mass is transported through the geological barrier, which can be considered as a conservative assumption. With a potentially lower recharge rate at the top of the landfill through sealing during the backfilling and water drainage extraction above the geological barrier, the concentration in the groundwater would be significantly lower (Artmann et al., 2020).

The different initial saturation conditions in DuMu^{x} are the reason for the deviations from the d^{3}f++ and SPRING concentration curves. Flow simulations were performed for d^{3}f++ and SPRING and the results were used as initial conditions for the saturation of the model compartments. In DuMu^{x}, the selected boundary conditions did not lead to a converging solution. For this reason, the initial saturation condition for the transport simulations was averaged from d^{3}f++ saturation results across the landfill and the result was used as the initial condition for saturation in DuMu^{x}. These differences in the initial conditions lead to different concentration curves at observation points P1 and P2. At P3, the tracer has already been transported through the unsaturated zone and parts of the aquifer. After just over 11 yr, the concentration in d^{3}f++ and SPRING is $0.54\,\mathrm{kg\,kg^{-1}}$, while in DuMu^{x} the maximum concentration is $0.38\,\mathrm{kg\,kg^{-1}}$. A slight time lag can be seen in the peaks in the d^{3}f++ results, compared to DuMu^{x} and SPRING. The transport of substances through the geological barrier and the aquifer is slightly faster in d^{3}f++. The concentration maxima of SPRING and DuMu^{x} occur at approximately the same time. In SPRING and DuMu^{x} the concentration maximum occurs about one and a half years later at observation point P3. A reason for the different concen-

https://doi.org/10.5194/sand-2026-11
Preprint. Discussion started: 16 June 2026

SaND
Safety of Nuclear Waste Disposal
Discussions

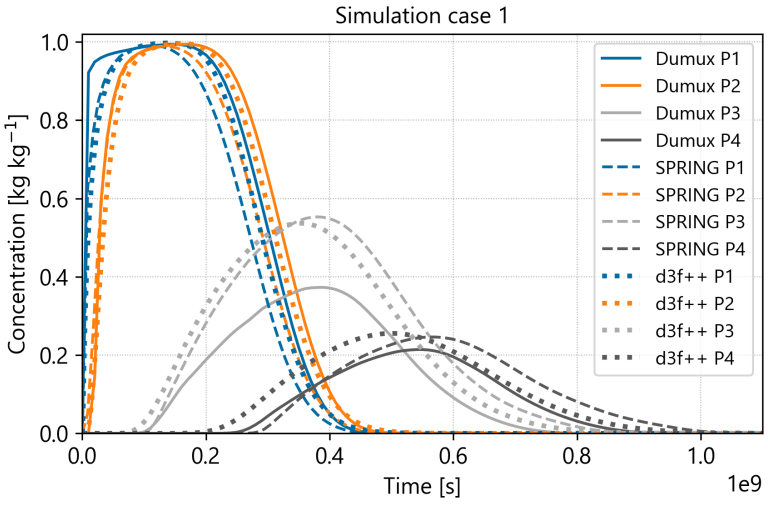

Figure 9. Concentration curves at the different observation points in the landfill model for simulation case 1 ($\alpha_l = 0.1\,\mathrm{m}$ and $K_d = 0\,\mathrm{m^3\,kg^{-1}}$) for the three different Codes DuMu^x (solid line), d^{3}f++ (dotted line) and SPRING (dashed line). Locations of the observation points are shown in Figure 2.

trations at P3 is the mass distribution in the aquifer and the dispersive flux. The results were also compared by visualizing the two-dimensional concentration plots. In DuMu^x the concentration plume is distributed stronger over the whole aquifer depth. In d^{3}f++ and SPRING the plume is focused stronger in the area of the observation point and leads to higher concentrations at P3.

SPRING simulates without the upwind method, whereas in d^{3}f++ stabilisation by upwind can be partially or fully activated. DuMu^x converges only with small time steps without the upwind method, so upwind was used here. In further simulations with d^{3}f++, upwind was also used to test the influence of upwind methods on the results. The results are shown in Figure A1 and are similar to the results of DuMu^x. The differences at observation point three can therefore be attributed to the stronger dispersion and the additional upwind method in DuMu^x. At observation point P4, the time lag of the maximum concentration becomes more prominent. The maximum concentration is first reached in d^{3}f++, about $3\,\mathrm{yr}$ before the peak in SPRING. In DuMu^x the peak is between the other two simulation code results.

In simulation cases 2 and 3, the dispersion coefficient is increased from $0.1\,\mathrm{m}$ to $1\,\mathrm{m}$ compared to simulation case 1. In the soil model, a dispersion coefficient of $1\,\mathrm{m}$ represents a high value in relation to the grid size, but in the landfill model this value may be quite realistic. Higher dispersion coefficients results in stronger concentration distribution in all model layers. None of the codes reaches a maximum concentration of $1\,\mathrm{kg\,kg^{-1}}$ at the four observation points.

In simulation case 2, DuMu^x shows the highest concentrations at observation points P1 and P2 and a slower discharge from the landfill into the aquifer, corresponding to the less steep concentration curve compared to SPRING and d^{3}f++ (Figure 10). These codes show lower concentrations at points P1 and P2 compared to DuMu^x, as for simulation case 1. The concentration curves

https://doi.org/10.5194/sand-2026-11
Preprint. Discussion started: 16 June 2026

for P1 and P2 are very similar for SPRING and d^{3}f++. In DuMu^x the concentration remains higher for a longer time period at P1 and P2 with a steeper curve gradient after the peak. At observation points P3 and P4, the higher dispersion coefficient leads to an equalisation of the concentrations of the various simulation codes compared to simulation case 1. Downstream, the concentration curves of all codes differ slightly, with an earlier peak in d^{3}f++, the highest concentration in SPRING and the lowest concentration in DuMu^x. The time difference between the maximum peak concentration is around 1 yr for the simulation cases 1 and 2 at P4 due to the higher sorption coefficient ($K_d = 1 \times 10^{-5}\,\mathrm{m^3\,kg^{-1}}$).

The results of simulation case 2 show no significant differences for the time of maximum concentration compared to simulation case 1, so dispersion has a small influence on the timing of the peak. However, the dispersion coefficient does have an influence on the concentration distribution and the concentration peak. Due to the stronger dispersion, the tracer is mixed more strongly with the fresh water from the aquifer. At observation point P3, the maximum concentration is lower compared to simulation case 1, while at observation point P4 the effect is less strong. With a smaller dispersion coefficient, the freshwater mixes with the groundwater less quickly than with a higher dispersion coefficient, so that at P3 the mixing for simulation case 1 is not yet as strong as in simulation case 2. Transport in the groundwater causes the tracer to mix increasingly with the fresh water, and at P4 the mixing is so advanced that the different dispersion coefficients do not make a significant difference.

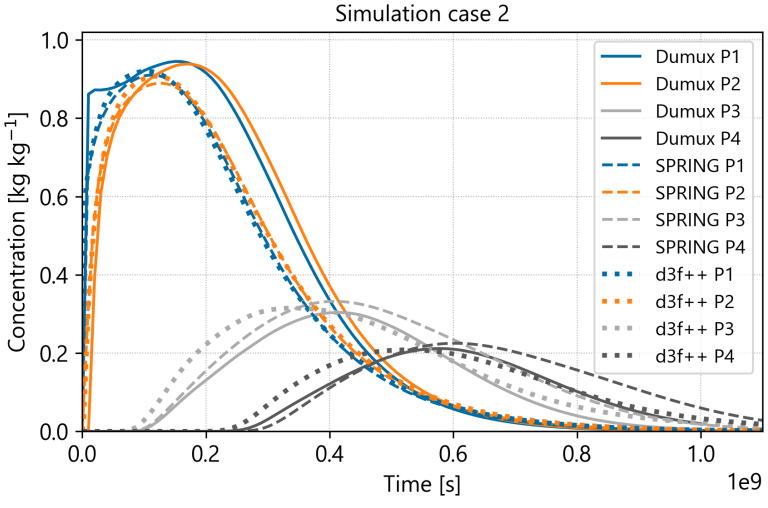

Figure 10. Concentration curves at the different observation points in the landfill model for simulation case 2 ($\alpha_l = 1\,\mathrm{m}$ and $K_d = 1 \times 10^{-5}\,\mathrm{m^3\,kg^{-1}}$) for the three different Codes DuMu^x (solid line), d^{3}f++ (dotted line) and SPRING (dashed line). Locations of the observation points are shown in Figure 2.

Simulation case 3 shows a stronger influence of the sorption coefficient (K_d) on the transport times through the model (Figure 11). The travel times are nearly doubled with concentration peaks for P4 after 35 yr instead of 18 yr before for DuMu^x. The trends regarding the codes remain the same even with increased sorption coefficients. The concentrations at P1 and P2 are highest in DuMu^x due to the modified initial saturation condition and increase to $1\,\mathrm{kg\,kg^{-1}}$ despite the higher dispersion

https://doi.org/10.5194/sand-2026-11
Preprint. Discussion started: 16 June 2026

SaND
Safety of Nuclear Waste Disposal
Discussions

coefficient. While the concentration curves in simulation case 2 for P1 and P2 were almost identical between d^{3}f++ and SPRING, d^{3}f++ now shows a slightly faster concentration peak as in the simulation cases 1 and 2 at the observations points P3 and P4.

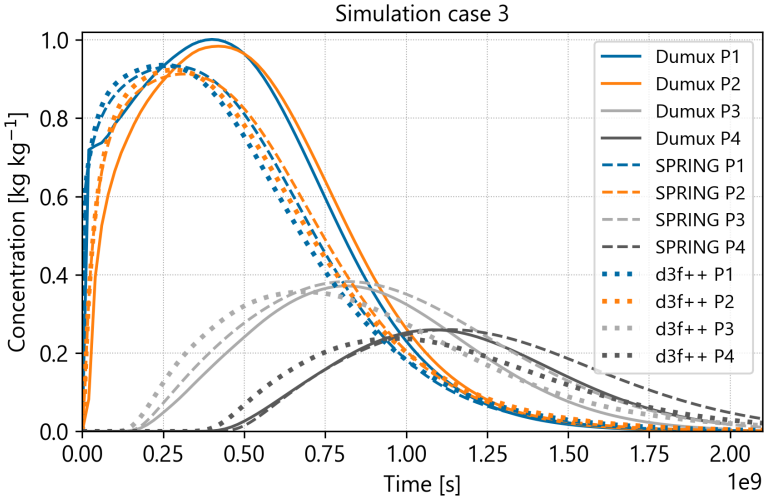

Figure 11. Concentration curves at the different observation points in the landfill model for simulation case 3 (α_l = 1 m and K_d = 1 × 10^{-4} m^3 kg^{-1}) for the three different Codes DuMu^x (solid line), d^{3}f++ (dotted line) and SPRING (dashed line). Locations of the observation points are shown in Figure 2.

5 Discussion

The topic of the disposal of decommissioning waste from nuclear power plants is becoming increasingly important due to the phase-out of nuclear energy in Germany in 2023. To ensure that the population is not exposed to any additional radiation doses, dose estimations are carried out for various disposal pathways. The IAEA's 10 μSv criterion must be respected in this process. The groundwater pathway beneath a landfill site is a possible contamination pathway. As only very small quantities of decommissioning waste have been disposed of in landfills to date, there are no calibration or validation options for the model simulations carried out here. The models and parameters are of generic origin. The focus of this work was on comparing the numerical groundwater flow and transport codes d^{3}f++, DuMu^x and SPRING.

This work has also shown that supposedly simple model geometries can lead to different simulation results in the three codes if the implementation of the flow and transport processes are not compared adequately. An initial comparison of codes using simple examples serves as a valuable approach for transparently identifying similarities and differences. The presented results show good agreement between the three numerical flow and transport codes. Differences in the results could be identified and attributed to individual processes or numerical factors like the upwind method and dispersion.

https://doi.org/10.5194/sand-2026-11
Preprint. Discussion started: 16 June 2026


SaND Safety of Nuclear Waste Disposal Discussions

This includes increased grid-dependent dispersion, which causes a greater distribution of concentration in the DuMu^x simulations with high dispersion coefficients for the grid size. Another difference is the implementation and use of upwind methods, which are not used in SPRING, can be switched on or off in d^{3}f++, and are necessary in DuMu^x for the solutions to converge well with some parameter combinations. As described in Section 4.2 the deviations in the concentration curves can be attributed to the averaged initial saturation conditions used in DuMu^x to reach a converging solution and the higher dispersion flux resulting in a lower concentration at observation point P3 because the concentration plume is more concentrated at this point in d^{3}f++ and SPRING. The differences between the FE and FV method of the simulation codes had no visible influence on the results. In d^{3}f++ and SPRING, saturation is calculated in initial flow simulations until a steady state is reached, and the saturation conditions calculated at the steady state are used as initial conditions for the transport simulations. In DuMu^x, such calculated flow conditions cannot be implemented in the same way as in d^{3}f++ and SPRING; therefore, the steady-state saturation from the d^{3}f++ simulations was averaged and used as the initial condition for the saturation conditions in the landfill, so that the amount of material remains comparable. The differing saturation distributions led to different concentration curves at the start of the transport simulation in DuMu^x. The differences are apparent in the steeper rise in concentration and the sharply changing concentration profile immediately after the start of the transport simulation in DuMu^x. The model assumptions were chosen to be as simple and conservative as possible in order to ensure good comparability of the codes. No drainage water extraction was assumed in the landfill model at the drainage layer, where a large part of the contamination would be discharged to a wastewater treatment plant. The entire amount of tracer is therefore transported through the landfill into the underlying groundwater under constant infiltration water. The sorption coefficients used in the landfill model are in the lower range of sorption coefficients, so significantly longer transport times are to be expected for most radionuclides. The comparison simulations show good overall agreement in the results, with differences attributable to individual processes and methods used in the codes.

6 Conclusions

Several numerical groundwater simulation cases were carried out in this work to compare the three codes d^{3}f++, DuMu^x and SPRING. A soil model and a landfill model were set up. As only very small quantities of decommissioning waste from nuclear facilities have been sent to landfill to date, there is no way of calibrating or validating the numerical models with real data. This code comparison was done to strengthen the trust and to identify differences in the implementation of mass transport processes in numerical simulation codes. In addition, parameter variation simulations were carried out for the two models in order to investigate the effects of parameter changes on tracer concentration.

The equation systems for the flow and transport processes were successfully compared with each other. Differences were identified in the description of sorption and tortuosity in the diffusion term, which were adjusted in DuMu^x for the simulations. The mass transport terms of advection, dispersion, diffusion, sorption and decay are mathematically implemented in the same way. The breakthrough curves for almost all simulation cases show good agreement for all three numerical simulation codes.

The transport times of contaminated soil in a soil column and from a landfill to groundwater depend primarily on the potential

https://doi.org/10.5194/sand-2026-11
Preprint. Discussion started: 16 June 2026

SaND
Safety of Nuclear Waste Disposal
Discussions

sorption capacity of the radionuclides. Transport parameters such as diffusion played a smaller role in these simulations in more permeable materials. Dispersion is more related to the grid size and model size and must be adjusted accordingly depending on the model size. The material properties and especially the radionuclides under consideration with their chemical characteristics have a major influence on transport behavior. The difficulty lies in determining the sorption coefficients for the radionuclides. In the model simulations shown here, different sorption coefficients were applied to demonstrate possible effects on transport times, with the focus on code comparison. A positive conclusion can be drawn from this comparison. The concentrations are within the same order of magnitude and the processes causing the deviations have been identified. The work has shown that a code comparison with a supposedly simple grid is necessary in order to reliably identify differences in the codes that could be obscured by different processes in more complex models. The investigations increase the robustness of numerical codes as a basis for simulating concentrations in the groundwater pathway, which can be used for later dose estimation in the future.

Appendix A: Tables with simulation cases and parameters

Table A1. Transport parameters for different simulation cases for the soil model.

Simulation case	saturated/ unsaturated	α_l [m]	α_t [m]	D_{eff}^{κ} [$m^2 s^{-1}$]	K_d [$m^3 kg^{-1}$]
1	saturated	0	0	0	0
2	saturated	0.1	0.01	0	0
3	saturated	0	0	1×10^{-9}	0
4	saturated	0	0	0	1×10^{-4}
5	saturated	0.1	0.01	1×10^{-9}	1×10^{-5}
6	saturated	0.1	0.01	1×10^{-9}	1×10^{-4}
7	saturated	0.1	0.01	1×10^{-9}	1×10^{-3}
8	saturated	1	0.1	1×10^{-9}	1×10^{-5}
9	saturated	1	0.1	1×10^{-9}	1×10^{-4}
10	saturated	1	0.1	1×10^{-9}	1×10^{-3}
11	unsaturated	0	0	0	0
12	unsaturated	0.1	0.01	0	0
13	unsaturated	0	0	1×10^{-9}	0
14	unsaturated	0	0	0	1×10^{-4}
15	unsaturated	0.1	0.01	1×10^{-9}	1×10^{-5}
16	unsaturated	0.1	0.01	1×10^{-9}	1×10^{-4}
17	unsaturated	0.1	0.01	1×10^{-9}	1×10^{-3}
18	unsaturated	1	0.1	1×10^{-9}	1×10^{-5}
19	unsaturated	1	0.1	1×10^{-9}	1×10^{-4}
20	unsaturated	1	0.1	1×10^{-9}	1×10^{-3}

https://doi.org/10.5194/sand-2026-11
Preprint. Discussion started: 16 June 2026

SaND
Safety of Nuclear Waste Disposal
Discussions

Table B1. Transport parameters for different simulation cases for the landfill model.

Simulation case	α_l m	α_t m	D^{κ}_{eff} $\mathrm{m^2\,s^{-1}}$	K_d $\mathrm{m^3\,kg^{-1}}$
1	0.1	0.01	1×10^{-9}	0
2	1	0.1	1×10^{-9}	1×10^{-5}
3*	1	0.1	1×10^{-9}	1×10^{-4}

* higher upwind value used in DuMu^{x} due to convergence issues

https://doi.org/10.5194/sand-2026-11
Preprint. Discussion started: 16 June 2026

SaND
Safety of Nuclear Waste Disposal
Discussions

Table C1. Boundary coordinates for the model design.

X [m]	Y [m]	Description
0	21.25	Aquifer bottom left
0	41.25	Aquifer surface left
50	40	Contact aquifer to barrier left
50	41	Contact barrier to drainage left
50	41.5	Contact drainage to landfill left
50	66.5	Landfill surface left
350	59	Landfill surface right
350	34	Contact drainage to landfill right
350	33.5	Contact barrier to drainage right
350	32.5	Contact aquifer to barrier right
850	20	Aquifer surface right
850	0	Aquifer bottom right

Appendix D: Additional breakthrough plots for different landfill models

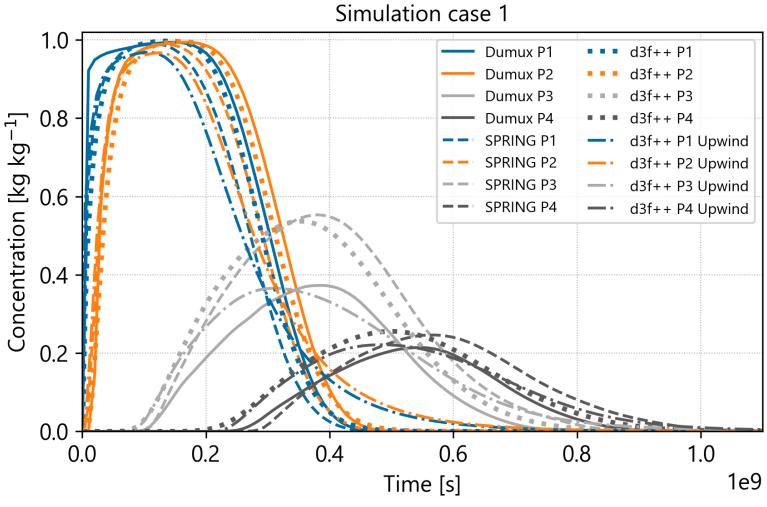

Figure A1. Landfill model concentration curves for simulation case 1 (α_l = 0.1 m and K_d = 0 m^3 kg^{-1}) with full upwind in d^{3}f++ at different observation points.

https://doi.org/10.5194/sand-2026-11
Preprint. Discussion started: 16 June 2026

SaND
Safety of Nuclear Waste Disposal
Discussions

Author contributions. Marc Johnen was responsible for the conceptualization, data curation, methodology, software, validation, visualization and writing of this article. Roman Winter worked on the conceptualization, data curation, methodology, software, validation, visualization and did the writing. Bernd Flemisch and Holger Class helped with the methodology and conceptualization, developed the software code, validation of the models and the writing as reviewers and several discussions. Holger Seher and Henrich Meyering are responsible for the base conceptualization of this project, the funding acquisition, project administration, supervision of the project and reviewing the article. All authors have read and approved the final version of the manuscript.

Competing interests. The authors declare that they have no financial or personal relationships that could be perceived as potential conflicts of interest regarding this research.

Acknowledgements. This project was funded by the Federal Ministry for the Environment, Climate Action, Nature Conservation and Nuclear Safety (BMUKN) (Funding reference number: 3622S72540). The views and conclusions expressed here are those of the authors and do not necessarily reflect the official position of the BMUKN. The authors would like to thank the Federal Ministry for the Environment, Climate Action, Nature Conservation and Nuclear Safety (BMUKN) for funding and the Federal Office for Radiation Protection (BfS) for the technical project support. Artificial intelligence (AI) (MS Copilot) was used in some cases for the scripts used to plot the results.

https://doi.org/10.5194/sand-2026-11
Preprint. Discussion started: 16 June 2026

SaND
Safety of Nuclear Waste Disposal
Discussions

References

Ahusborde, E., Amaziane, B., and Jurak, M.: 3D numerical simulation by upscaling of gas migration through engineered and geological barriers for a deep repository for radioactive waste, Tech. rep., LMA Pau, 2015.

Artmann, A., Eberhard, H., Filby, A., Hussels, M.-T., Johnen, M., Seher, H., Thielen, H., and Weyand, T.: Freigabekonzepte einer neuen Strahlenschutzverordnung nach Euratom- Grundnormen 2013 in der Anwendung, vol. GRS-506, Gesellschaft für Anlagen- und Reaktorsicherheit (GRS) gGmbH, ISBN 978-3-946607-91-5, 2020.

Bastian, P., Blatt, M., Dedner, A., Dreier, N.-A., Engwer, C., Fritze, R., Gräser, C., Grüninger, C., Kempf, D., Klöfkorn, R., Ohlberger, M., and Sander, O.: The Dune framework: Basic concepts and recent developments, Computers & Mathematics with Applications, 81, 75–112, https://doi.org/https://doi.org/10.1016/j.camwa.2020.06.007, development and Application of Open-source Software for Problems with Numerical PDEs, 2021.

Benson, C., Chiang, I., Chalermyanont, T., and Sawangsuriya, A.: Estimating van Genuchten Parameters α and n for Clean Sands from Particle Size Distribution Data, in: Estimating van Genuchten Parameters α and n for Clean Sands from Particle Size Distribution Data, pp. 410–427, ISBN 978-0-7844-1326-5, https://doi.org/10.1061/9780784413265.033, 2014.

Bundesrepublik Deutschland: Verordnung über Deponien und Langzeitlager: Deponieverordnung - DepV, 2024.

Class, H., Bürkle, P., Sauerborn, T., Trötschler, O., Strauch, B., and Zimmer, M.: On the role of density-driven dissolution of CO_2 in phreatic karst systems, Water Resources Research, 57, https://doi.org/10.1029/2021WR030912, 2021.

delta h: SPRING Benutzerhandbuch - Die Software für die professionelle Gewässersystemmodellierung, Tech. rep., delta h, ISBN 9783000734335, https://spring.delta-h.de, 2024.

Deutscher Bundestag: Gesetz über die friedliche Verwendung der Kernenergie und den Schutz gegen ihre Gefahren: Atomgesetz - AtG, 2022.

Deutscher Bundestag: Gesetz zum Schutz vor der schädlichen Wirkung ionisierender Strahlung (Strahlenschutzgesetz): StrlSchG, 2024a.

Deutscher Bundestag: Verordnung zum Schutz vor der schädlichen Wirkung ionisierender Strahlung: Strahlenschutzverordnung - StrlSchV, 2024b.

Fein, E.: Software Package r3t : Model for Transport and Retention in Porous Media: Final Report, vol. GRS-192, Gesellschaft für Anlagen- und Reaktorsicherheit (GRS) gGmbH, ISBN 3931995607, 2004.

Fein, E. and Schneider, A.: d3f - Ein Programmpaket zur Modellierung von Dichteströmungen, vol. GRS-139, Gesellschaft für Anlagen- und Reaktorsicherheit (GRS) gGmbH, ISBN 3923875975, 1999.

Flemisch, B., Darcis, M., Erbertseder, K., Faigle, B., Lauser, A., Mosthaf, K., Müthing, S., Nuske, P., Tatomir, A., Wolff, M., and Helmig, R.: DuMux: DUNE for multi-phase,component,scale,physics,... flow and transport in porous media, Advances in Water Resources, 34, 1102–1112, https://doi.org/https://doi.org/10.1016/j.advwatres.2011.03.007, new Computational Methods and Software Tools, 2011.

Flügge, J., Fahrenholz, C., Schönwiese, D., Seher, H., and Johnen, M.: Auswirkungen von Subrosion auf die Barrierewirkung des ewG und des Deckgebirges eines potenziellen Endlagerstandorts für hochradioaktive Abfälle: Synthesebericht, vol. GRS-801, Gesellschaft für Anlagen- und Reaktorsicherheit (GRS) gGmbH, ISBN 978-3-910548-94-7, 2024.

International Atomic Energy Agency (IAEA): Principles for the Exemption of Radiation Sources and Practices from Regulatory Control, Tech. rep., International Atomic Energy Agency (IAEA), Vienna, ISBN 9201238886, 1988.

https://doi.org/10.5194/sand-2026-11
Preprint. Discussion started: 16 June 2026

Koch, T., Gläser, D., Weishaupt, K., et al.: DuMux 3 – an open-source simulator for solving flow and transport problems in porous media with a focus on model coupling, Computers & Mathematics with Applications, 81, 423–443, https://doi.org/10.1016/j.camwa.2020.02.012, 2021.

LH2: Dumux Handbook, Tech. rep., IWS - Universität Stuttgart, http://dumux.org, 2024.

Merk, R.: Numerical modeling of the radionuclide water pathway with HYDRUS and comparison with the IAEA model of SR 44, Journal of Environmental Radioactivity, 105, 60–69, https://doi.org/10.1016/j.jenvrad.2011.10.014, 2012.

Nayagum, D., Schäfer, G., and Mosé, R.: Modelling Two-Phase Incompressible Flow in Porous Media Using Mixed Hybrid and Discontinuous Finite Elements, Computational Geosciences, 8, 49–73, https://doi.org/10.1023/B:COMG.0000024446.98662.36, 2004.

Nordbotten, J. M., Flemisch, B., Gasda, S. E., Nilsen, H. M., Fan, Y., Pickup, G. E., Wiese, B., Celia, M. A., Dahle, H. K., Eigestad, G. T., and Pruess, K.: Uncertainties in practical simulation of CO2 storage, International Journal of Greenhouse Gas Control, 9, 234–242, https://doi.org/10.1016/j.ijggc.2012.03.007, 2012.

Noseck, U., Brendler, V., Britz, S., Stockmann, M., Fricke, Julian Richter, C., Lampe, M., Gehrke, A., and Flügge, J.: Smart Kd-Concept for Long-term Safety Assessments, vol. GRS-500, Gesellschaft für Anlagen- und Reaktorsicherheit (GRS) gGmbH, ISBN 978-3-946607-85-4, 2018.

Rübel, A. and Gehrke, A. C.: Modellierung des Radionuklidtransports im Tongestein: Aktualisierung der Sicherheits- und Nachweismethodik für die HAW-Endlagerung im Tongestein in Deutschland, vol. GRS-668, Gesellschaft für Anlagen- und Reaktorsicherheit (GRS) gGmbH, ISBN 978-3-949088-59-9, 2022.

Scheidegger, A.: General Theory of Dispersion in Porous Media, Journal of Geophysical Research, 66, https://doi.org/10.1029/JZ066i010p03273, 1961.

Schneider, A., Wolf, J., and Zhao, H.: Projekt go-CAM: Implementierung strategischer Entwicklungsziele im Küstenzonenmanagement, Teilvorhaben 2: Grundwasserströmung und Schadstoffstransport : Schlussbericht, vol. GRS-660, Gesellschaft für Anlagen- und Reaktorsicherheit (GRS) gGmbH, ISBN 978-3-949088-51-3, 2022.

Seher, H., Navarro, M., Artmann, A., Larue, J., Roloff, R., and Weiß, D.: Modelling contaminant transport in generic landfills for decommissioning waste from German nuclear power plants, Progress in Nuclear Energy, 89, 46–56, https://doi.org/https://doi.org/10.1016/j.pnucene.2016.01.015, 2016.

Sheppard, M. I. and Thibault, D. H.: Default soil solid/liquid partition coefficients, Kds, for four major soil types: a compendium, Health Physics, 54, 471–482, 1990.

Šimůnek, J., Jarvis, N. J., Van Genuchten, M. T., and Gärdenäs, A.: Review and comparison of models for describing non-equilibrium and preferential flow and transport in the vadose zone, Journal of Hydrology, 272, 14–35, https://doi.org/10.1016/S0022-1694(02)00252-4, 2003.

Stockmann, M., Schikora, J., Becker, D.-A., Flügge, J., Noseck, U., and Brendler, V.: Smart Kd-values, their uncertainties and sensitivities - Applying a new approach for realistic distribution coefficients in geochemical modeling of complex systems, Chemosphere, 187, 277–285, https://doi.org/https://doi.org/10.1016/j.chemosphere.2017.08.115, 2017.

Strahlenschutzkommission: Freigabe von Stoffen zur Beseitigung, 2006.

Suilmann, J., Tischner, T., and Graf, T.: Improving geothermal doublet efficiency in multiple sandstone horizons in Hannover/Germany, Grundwasser, 30, 3–18, https://doi.org/10.1007/s00767-024-00585-6, 2025.

https://doi.org/10.5194/sand-2026-11
Preprint. Discussion started: 16 June 2026

Thierfeldt, S. and Wörlen, S.: Spezifische Fragestellungen für die Fortentwicklung von Datensätzen für die Freigrenzen, Freigabe von Oberflächenkontaminationen. Fortentwicklung des radiologischen Modells für die Berechnung von Freigabewerten für die Freigabe zur Beseitigung: Ergänzungen und Durchsicht: 17. Dezember 2004, 2004.

United States Environmental Protection Agency (US EPA): Understanding variation inpartition coefficient, Kd, values - Volume I: The Kd Model, Methods of Measurement, and Application of Chemical Reaction Codes, Tech. rep., United States Environmental Protection Agency (US EPA), Washington, 1999.

van Genuchten, M. T.: A Closed-form Equation for Predicting the Hydraulic Conductivity of Unsaturated Soils, Soil Science Society of America Journal, 44, 892–898, https://doi.org/10.2136/sssaj1980.03615995004400050002x, 1980.

Winter, R., Valsamidou, A., Class, H., and Flemisch, B.: A Study on Darcy versus Forchheimer Models for Flow through Heterogeneous Landfills including Macropores, Water, 14, https://doi.org/10.3390/w14040546, 2022.